Research Square

Preprints are preliminary reports that have not undergone peer review.
They should not be considered conclusive, used to inform clinical practice,
or referenced by the media as validated information.

The dynamical advantage of scale-free networks

Huijun Gao

hjgao@hit.edu.cn

Harbin Institute of Technology https://orcid.org/0000-0003-1865-7492

Yimeng Qi

Harbin Institute of Technology

Songlin Zhuang

Yongjiang Laboratory https://orcid.org/0000-0003-3072-0634

Zhihong Zhao

Ningbo University of Technology

Xiaotian Lin

Yongjiang Laboratory

Xinghu Yu

Ningbo Institute of Intelligent Equipment Technology Company Limited

Weichao Sun

Harbin Institute of Technology

Fangzhou Liu

Harbin Institute of Technology https://orcid.org/0000-0002-1275-4809

Charo I. del Genio

Trakia University

Baruch Barzel

Bar-Ilan University https://orcid.org/0000-0001-8862-4384

Stefano Boccaletti

CNR https://orcid.org/0000-0002-5758-7012

Article

Keywords:

Posted Date: September 1st, 2026

DOI: https://doi.org/10.21203/rs.3.rs-10546519/v1

License: This work is licensed under a Creative Commons Attribution 4.0 International License.
Read Full License

Additional Declarations: There is **NO** Competing Interest.

The dynamical advantage of scale-free networks

Yimeng Qi[1,*], Songlin Zhuang[2,*], Zhihong Zhao[3,*], Xiaotian Lin[2], Xinghu Yu[4], Weichao Sun[1], Fangzhou Liu[1,†], Charo I. del Genio[5], Baruch Barzel[6,7], Huijun Gao[1,†], Stefano Boccaletti[3,8,9]

1. Research Institute of Intelligent Control and Systems, Harbin Institute of Technology, Harbin 150001, China
2. Yongjiang Laboratory, Ningbo 315202, China
3. Institute of Interdisciplinary Intelligent Science, Ningbo Univ. of Technology, Ningbo, China
4. Ningbo Institute of Intelligent Equipment Technology Company Limited, Ningbo 294221, China
5. Institute of Smart Agriculture for Safe and Functional Foods and Supplements, Trakia University, Stara Zagora 6000, Bulgaria
6. Department of Mathematics, Bar-Ilan University, Ramat-Gan, Israel
7. The Gonda Multidisciplinary Brain Research Center, Bar-Ilan University, Ramat-Gan, Israel
8. Sino-Europe Complex Science Center, North University of China, Shanxi, Taiyuan 030051, China
9. CNR – Institute of Complex Systems, I-50019 Sesto Fiorentino, Italy

* These authors contributed equally to this work.

† Corresponding authors: fangzhou.liu@hit.edu.cn; hjgao@hit.edu.cn

Degree heterogeneity, a hallmark of complex networks, reflects a universal structural principle observed across diverse natural and technological systems. It is known to confer remarkable structural robustness against node or link removal, but does this pervasive feature also shape a system's dynamical functionality? To address this question, we use control theory to examine how degree heterogeneity influences a network's controllability profile. Previous work has shown that heterogeneous networks are generally difficult to control. Here, however, we demonstrate that this conclusion depends critically on the control target. When the objective is to drive the system toward an arbitrary dynamical state, heterogeneity indeed hinders controllability. Yet when the target lies on one of the system's natural attractors, the picture reverses and degree heterogeneity becomes a facilitator of controllability. We interpret this as evidence that heterogeneity enhances a system's functional robustness, making the network selective: it resists being driven toward arbitrary states, while remaining highly responsive to signals that guide it toward its innate dynamical attractors. Degree heterogeneity therefore emerges not only as a structural hallmark of complex systems, but also as a dynamical design principle that balances stable functionality with external controllability.

Complex networks – social, biological, and technological – often exhibit extreme levels of heterogeneity [1]. Many display fat-tailed, often scale-free, degree distributions [2,3], a phenomenon observed across diverse systems, including metabolic networks [4], gene regulation [5], protein interactions [6], communication systems [7], social networks [8], financial systems [9], and the brain [10]. It therefore represents a universal structural feature of networks, whose emergence transcends the specific mechanisms of any particular domain [11].

This prompts a fundamental question, why do networks trend toward such extreme heterogeneity? Is this merely an empirical observation, or does this phenomenon offer unique functional advantages to a complex system?

Over the years, this question has been addressed from multiple perspectives. Early on, the Barabási-Albert model proposed a universal mechanism for the emergence of scale-freeness [2]. Based on network growth and preferential attachment, the model explained how degree heterogeneity arises and why it is so prevalent. However, it offered little insight into the functional role of these exotic network structures. Such insights into the intrinsic advantages of degree heterogeneity emerged soon after. Networks with a fat-tailed degree distribution were shown to be

remarkably robust to random failures[12–14]. The hubs, although rare, help hold the network together, forming a resilient backbone that enables the system to withstand substantial structural perturbations.

These observations concern the structural robustness of networks, but do not address their dynamical functionality. Capturing functionality requires characterizing the network's response to external inputs or perturbations[15]. Such inputs, whether naturally occurring or artificially imposed, may steer the system between states, thereby altering its function even when the underlying structure remains intact[16,17]. On this front, two established approaches appear to yield contrasting conclusions. Structural controllability theory[18–20] indicates that scale-free networks are difficult to control, as they require a large number of driver nodes to steer the system between arbitrary dynamical states. By contrast, targeting – the process of steering a system toward a desired trajectory – was shown to benefit from network heterogeneity[21]. Here, we place these two results within a unified framework. We show that they describe distinct control tasks, differentiated by the dynamical admissibility of the target state, and that together they reveal a crucial advantage conferred by network heterogeneity.

The classical controllability framework focuses on driving a system between arbitrary dynamical states $\mathbf{x}(0)$ and $\mathbf{x}(t)$. While this is a natural formulation for linear dynamics, it does not account for a defining feature of nonlinear systems: their unforced dynamics support only a restricted repertoire of attractors and recurrent trajectories that represent the system's intrinsic modes of operation[22–24]. We therefore distinguish between arbitrary targets, representing any possible configuration, and *compatible targets*, defined as states or trajectories supported by the system's unforced dynamics and robustly generated from a basin of initial conditions. Compatible targets are thus part of the system's ingrained dynamical repertoire and, as such, may exhibit a distinct control profile.

With this distinction in mind, we move beyond the classical controllability paradigm, which seeks full control from any $\mathbf{x}(0)$ to any $\mathbf{x}(t)$, and partition control into two fundamentally different tasks according to the nature of the target state $\mathbf{x}(t)$. Incompatible control seeks to push the system outside its natural dynamical repertoire, effectively attempting to *reprogram* the network's intrinsic functionality. Compatible control, corresponding to targeting, instead steers the system toward states or trajectories supported by its intrinsic dynamics (Fig. 1).

We show that heterogeneous networks are indeed resistant to incompatible control, consistent with the predictions of the classical control paradigm. At the same time, however, they are highly amenable to compatible control. Hence, heterogeneous networks are selectively controllable: naturally inclined to return to their compatible states, while strongly resistant to arbitrary states that venture outside their functional domain. By analyzing both the size of the driver node set and the required control energy, we show that this selectivity increases systematically with network heterogeneity.

Consequently, degree-heterogeneous networks are not only structurally robust, but also *functionally robust* – exhibiting an intrinsic tendency to recover their designated functionality, alongside a marked resistance to being driven away from it. This reveals a clear *dynamical* advantage rooted in degree heterogeneity, and suggests a possible explanation for its widespread prevalence across diverse domains.

Results

Analysis framework. Consider a set $V = \{1, \dots, N\}$ of components (nodes), linked through a complex network A_{ij}, with degree distribution $P(k)$, average degree $\langle k \rangle$, and degree variance σ_k^2. Each node $i \in V$ is characterized by a d-dimensional dynamical state $\mathbf{x}_i(t) \in \mathbb{R}^d$. Hence, the *network* state is captured by the $N \times d$ dimensional $\mathbf{x}(t) = (\mathbf{x}_1(t), \dots, \mathbf{x}_N(t))^\top$.

The states $\mathbf{x}(t)$ evolve in time according to

$$\frac{\mathrm{d}\mathbf{x}}{\mathrm{d}t} = \mathbf{F}\big(\mathbf{x}(t)\big) + \mathbf{G}\big(\mathbf{x}(t), A\big) + B\mathbf{u}(t), \tag{1}$$

where $\mathbf{F}(\mathbf{x}(t))$ represents the nodal self-dynamics in the absence of interactions, and $\mathbf{G}(\mathbf{x}(t), A)$ captures the interaction mechanisms between adjacent nodes, as dictated by the network topology A. The control inputs $\mathbf{u}(t)$ are external signals applied to a subset of driver nodes $S \subseteq V$ via the binary input matrix B. The size of the driver node set is therefore

$$|S| = \sum_{i=1}^{N} \sum_{j=1}^{M} B_{ij} \tag{2}$$

where N and M are the numbers of rows and columns in B, respectively.

In the absence of external inputs, setting $S = \emptyset$ ($|S| = 0$), the system evolves along one of its *natural* dynamical trajectories $\mathbf{x}(t)$. The specific form of this trajectory depends on the initial condition $\mathbf{x}(t = 0)$, however, once the initial condition is fixed, the trajectory emerges as an intrinsic dynamical characteristic of (1).

In the limit $t \to \infty$, all natural trajectories asymptotically converge to one of the system's dynamical attractors. Together, these attractors define the system's *natural dynamical manifold* $\mathcal{M}$, a set of time-dependent solutions toward which (1) is naturally driven. We therefore view all dynamical trajectories $\mathbf{x}(t) \in \mathcal{M}$ as natural states, compatible with the system's intrinsic functionality. In contrast, trajectories $\mathbf{x}(t) \notin \mathcal{M}$ represent incompatible states, lying outside the domain of the system's functional landscape (Fig. 1b,c).

Controllability. In the classical controllability framework, the goal is complete control over the system's dynamics – to steer it from any arbitrary initial state $\mathbf{x}(0)$ to any desired final state $\mathbf{x}(t)$, whether within or outside $\mathcal{M}$. However, the distinction between compatible and incompatible states prompts a separation into two fundamentally different forms of control, depending on the nature of $\mathbf{x}(t)$:

Compatible control – targeting. In compatible control, the target state $\mathbf{x}(t)$ is not arbitrary but resides within $\mathcal{M}$, and hence belongs to the domain of (1)'s built-in functionality. This form of control aims to place the system on track toward one of its natural attractor states. After an initial control phase, once the system is brought into the basin of attraction of the desired state, the control inputs can be relaxed, allowing the system to evolve autonomously toward $\mathbf{x}(t)$.

Incompatible control. Here the goal is to force the system along an arbitrary trajectory $\mathbf{x}(t) \notin \mathcal{M}$ (or $\mathbf{x}(t) \in \overline{\mathcal{M}}$), thereby driving it outside the domain of its natural functionality. It requires an initial steering phase followed by an indefinite maintenance phase, during which external inputs $\mathbf{u}(t)$ must continuously counteract the system's intrinsic restoring forces that pull it back toward $\mathcal{M}$.

Hence, in line with the existing terminology, control, in its classic definition, describes the process of driving the system toward any final state $\mathbf{x}(t)$, compatible or incompatible (Fig. 1a). Our division partitions all control tasks into two subsets: incompatible control when $\mathbf{x}(t) \in \overline{\mathcal{M}}$ (Fig. 1b); compatible control for when $\mathbf{x}(t) \in \mathcal{M}$ (Fig. 1c). Compatible control is equivalent to what is often referred to in the literature as targeting[25,26].

Conceptually, these two control objectives can be visualized as motion on a rugged landscape. States within $\mathcal{M}$ form valleys and basins (blue), while states outside $\mathcal{M}$ lie on ridges and peaks (red). Compatible control exploits the landscape geometry, nudging the system into a favorable basin and then releasing it to follow its natural dynamics. In contrast, incompatible control works against the landscape, attempting to constrain the system on an unstable ridge or peak (Fig. 1d,e).

Functional robustness. A system is considered functionally robust if it is highly responsive to compatible control but strongly resistant to incompatible control. Such a system remains firmly confined within its intrinsic dynamical landscape $\mathcal{M}$, while resisting external attempts to drive it outside its functional domain. In natural ecological, social, and biological systems, as well as in complex engineered systems, functional robustness is highly desirable. It ensures that the system sustains a limited set of admissible behaviors and cannot be easily driven toward arbitrary, potentially dysfunctional states.

To quantify a system's functional robustness, we introduce two parameters that characterize control difficulty. The first is the minimal driver node set

$$S_{\min} = \underset{S \subseteq V}{\operatorname{argmin}} \left\{ |S| \;\middle|\; f\big(B, \mathbf{x}(0), \mathbf{x}(t)\big) = 1 \right\}, \tag{3}$$

which quantifies the smallest number of components that must be controlled to steer the system from $\mathbf{x}(0)$ to $\mathbf{x}(t)$. In (3), $|S|$ is taken from (2), and the function $f(B, \mathbf{x}(0), \mathbf{x}(t)) = 1$ if B is sufficient for the $\mathbf{x}(0) \to \mathbf{x}(t)$ control task, and zero otherwise. The minimization therefore identifies the subset S that achieves the desired control with the fewest driver nodes. We define $s = |S_{\min}|/N$ as the fraction of driver nodes, ranging from $s \to 0$ for an easily controllable system to $s = 1$ for extreme control difficulty, where all nodes must be directly controlled to reach the target state.

The second parameter is the control energy

$$E = \int_0^t ||\mathbf{u}(t')||^2 \, \mathrm{d}t', \tag{4}$$

expended along the trajectory from $\mathbf{x}(0)$ to $\mathbf{x}(t)$. In Supplementary Section 2.3, we also discuss the maintenance energy required to sustain the system at $\mathbf{x}(t)$, which is particularly relevant for incompatible control.

A functionally robust system is therefore characterized by small s and E for compatible control, together with large s and E for incompatible control, reflecting an intrinsic attraction to $\mathcal{M}$, alongside a strong resistance to excursions outside of it, and into $\overline{\mathcal{M}}$.

Note that, in principle, s and E depend on $\mathbf{x}(0)$ and $\mathbf{x}(t)$. For example, if $\mathbf{x}(0)$ lies close to $\mathbf{x}(t)$, control is expected to be more accessible, with s and E relatively small. Thus, $s = s(\mathbf{x}(0), \mathbf{x}(t))$ and $E = E(\mathbf{x}(0), \mathbf{x}(t))$. However, our focus here is not on a specific control trajectory, but rather on the typical, or expected, values of s and E, conditioned on whether $\mathbf{x}(t) \in \mathcal{M}$ or not. For notational simplicity, we therefore write s and E throughout, omitting the explicit dependence on $\mathbf{x}(0)$ and $\mathbf{x}(t)$.

Testing ground (Fig. 2). To systematically examine the functional robustness of complex systems we consider three canonical dynamical models: the Kuramoto dynamics of coupled one-dimensional oscillators (Fig. 2b, $d = 1$), and the Rössler and Lorenz systems, both employing three-dimensional ($d = 3$) dynamical units (Fig. 2c,d).

We implement each of these dynamics on a set of synthetic and real-world complex networks (Fig. 2a). The first five are homogeneous networks, incorporating a bounded $P(k)$ (blue-shaded). These include an Erdős-Rényi random graph (ER), a Watts-Strogatz small world network (SW), and three random networks with exponential (Exp), normal (Norm) and uniformly (Uni) distributed degrees. To these we add three heterogeneous scale-free networks, in which $P(k) \sim k^{-\gamma}$, with scaling exponents $\gamma = 3$ (SF1), $\gamma = 2.5$ (SF2) and $\gamma = 2$ (SF3), capturing increasing levels of degree heterogeneity.

Alongside these synthetic networks, we also considered empirical networks from distinct domains: Brain 1 [27] and Brain 2 [28], both derived from the human connectome, represent physical networks reconstructed from diffusion magnetic resonance imaging (dMRI). Their nodes correspond to distinct anatomical regions or voxels, while their links encode the white-matter fiber tracts connecting them. For Brain 1, whose full scale is of the order of 10^6 nodes, we extracted a sub-network of $N = 5,000$ nodes and $L = 78,500$ links, enabling scalable dynamical simulations. For Brain 2, a consensus connectome aggregating structural data across multiple healthy individuals, we used the complete network, with $N = 1,015$ and $L = 71,604$. We additionally considered Power 1 [29] and Power 2 [30]: the former maps the high-voltage topology of the Western United States power grid ($N = 4,941, L = 6,594$), while the latter is a benchmark grid from the Harwell-Boeing collection ($N = 5,300, L = 8,271$).

Among these empirical networks, Brain 1 and Brain 2 are naturally heterogeneous, exhibiting a fat-tailed $P(k)$, and therefore complement SF1, SF2 and SF3 in our heterogeneous network ensemble. Power 1 and Power 2, by contrast, are comparatively homogeneous. Finally, to isolate the impact of the ingrained degree heterogeneity of the two brain networks, we also constructed a homogeneous counterpart for each, obtained by randomly rewiring all links. This procedure preserves the network density while driving $P(k)$ toward a Poisson distribution.

Together, we arrive at a broad testing ground, comprising 16 networks of diverse scale and levels of heterogeneity. Each of these networks is examined against our three distinct types of dynamics, for a total of 48 systems upon which we examine functional robustness.

Experimental design. For each of our 48 systems, we examine both compatible and incompatible control, and map their functional robustness by measuring s and E, in view of their degree heterogeneity:

Kuramoto. For the Kuramoto system, the natural state space is the synchronization manifold $\mathcal{M}$. We initiate the system at an arbitrary state $\mathbf{x}(0)$ outside this manifold and designate two target states – the compatible $\mathbf{x}_{\mathrm{C}}(t)$ and the incompatible $\mathbf{x}_{\mathrm{IC}}(t)$. For $\mathbf{x}_{\mathrm{C}}(t)$, we consider the phase-locked solution, within $\mathcal{M}$ (Fig. 2e); for $\mathbf{x}_{\mathrm{IC}}(t)$, we force the system to the globally static state $\mathbf{x} = 0$ (Fig. 2f), which is unsupported by the system's natural dynamics.

Lorenz (Fig. 2g-h). For coupled Lorenz oscillators, $\mathcal{M}$ is given by the Lorenz attractor. We initiate the system at an arbitrary $\mathbf{x}(0)$, then apply control to guide it toward $\mathbf{x}_{\mathrm{C}}(t)$ along the attractor, or toward $\mathbf{x}_{\mathrm{IC}}(t)$, which we set as the static state $\mathbf{x}_{\mathrm{IC}}(t) = 0$ (Fig. 2h, red point).

Rössler (Fig. 2i-j). A similar scheme is used for the Rössler system. The compatible state $\mathbf{x}_{\mathrm{C}}(t)$ lies on the system's natural attractor, while the incompatible state $\mathbf{x}_{\mathrm{IC}}(t)$ is set at the origin (red dot), a forced pinning outside of $\mathcal{M}$.

Driver node set

We begin by examining the minimal driver node set $S_{\min}$ as defined in (3), under compatible and incompatible control, focusing on the impact of network structure, particularly degree heterogeneity.

Incompatible control. Incompatible control entails driving the system toward an arbitrary $\mathbf{x}(t)$. Therefore, the minimal driver node set corresponds to that of the classic structural controllability problem. In this setting, $S_{\min}$ is independent of the dynamics and of the specific states $\mathbf{x}(0)$ and $\mathbf{x}(t)$, being determined entirely by the network structure. Specifically, for a given network A, Eq. (1) is structurally controllable if the input matrix B satisfies the Kalman rank condition, which requires that the controllability matrix $C = [B, AB, A^2B, \ldots, A^{N-1}B]$ has full rank[31]. This is expressed in (3) by setting $f(B) = 1$ if Rank(C) = N, and $f(B) = 0$ if Rank(C) < N.

Therefore, under incompatible control we write

$$S_{\min}^{\mathrm{IC}} = \underset{S\subseteq V}{\operatorname{argmin}} \Big\{ |S| \;\Big|\; \mathrm{Rank(C)} = \mathrm{N} \Big\}, \tag{5}$$

seeking the minimal set of nodes for which the Kalman condition is fulfilled. To find this minimal set we use the maximum matching algorithm[18,32], whereby all unmatched nodes must be included in $S_{\min}^{\mathrm{IC}}$.

With this we can now extract the minimal driver node set directly for each of the 16 networks in our testing ground. Results for two specific networks – ER and SF1 – are shown in Fig. 3a,c (red nodes). In ER the fraction of driver nodes is $s = 0.49$; in SF1 it is $s = 0.61$. Hence, when it comes to incompatible control ER is easier to manipulate than SF1.

This observation is not unique to this particular pair of networks. In Fig. 3e we show the fraction of driver nodes s across the entire network ensemble, revealing a consistent trend: homogeneous network, such as ER, Uni, SW and Norm, are characterized by smaller s than the heterogeneous SF1, SF2, SF3 or Brain 1,2. They are therefore more easily controllable than their heterogeneous counterparts.

This result is no surprise. The fact that heterogeneity hinders controllability is well established and stems from the tendency of $S_{\min}^{\mathrm{IC}}$ to favor peripheral nodes while avoiding hubs. Indeed, a peripheral node is far more likely to become unmatched than a highly connected node. To illustrate this, in Fig. 3b,d we show $P(i \in S_{\min}^{\mathrm{IC}} \mid k_i)$, the probability that node i is included in the driver node set conditional on its degree k_i. As expected, this probability declines with k_i, indicating that controllability is negatively correlated with node degree. This is also observed, visually, in Fig. 3a,c: while the network layout condenses the hubs around the center, the control nodes (red) tend to favor the periphery.

This observed hub-avoidance arises from the fact that, under incompatible control, we aim to steer the system away from its natural dynamic manifold. This requires exerting control primarily over the low-degree nodes, whose states would otherwise naturally drift toward $\mathcal{M}$. In this scenario, the scale-free topology becomes a disadvantage: although the network is dominated by a small set of hubs, controlling its dynamics requires directly manipulating the overwhelming majority of low-degree nodes.

The crucial point is that this result applies to general controllability, where the goal is to push the system toward an arbitrary $\mathbf{x}(t)$, and specifically here to $\mathbf{x}(t) \in \overline{\mathcal{M}}$. If, however, we restrict ourselves to $\mathbf{x}(t) \in \mathcal{M}$, the *intuitive* insight above is inverted. Once the hubs are set on course toward the desired attractor, the peripheral nodes follow naturally, guided by the system's internal dynamics. To demonstrate this, we next determine $S_{\min}^{\mathrm{C}}$ for compatible control.

Compatible control. The driver node set in (5) can, in principle, steer the system to any desired target state, whether compatible or incompatible. However, if we specifically target compatible states, we anticipate a different driver node set, as control is now assisted by the natural dynamics of (1).

To construct $S_{\min}^{\mathrm{C}}$ for compatible control, consider a system of the form (1) at an initial state $\mathbf{x}(0)$ that we wish to bring into $\mathbf{x}(t) \in \mathcal{M}$. If $\mathbf{x}(0)$ is already within $\mathbf{x}(t)$'s basin of attraction $\beta_{\mathbf{x}(t)}$, no inputs $\mathbf{u}(t)$ are required. The system will reach the target state autonomously, and consequently $S_{\min}^{\mathrm{C}} = \emptyset$.

If, however, $\mathbf{x}(0) \notin \beta_{\mathbf{x}(t)}$, we seek inputs $\mathbf{u}(t)$ that drive it closer to the desired basin. This is captured by the maximum Lyapunov exponent (MLE) λ (Fig. 4a)[33,34]. Outside $\beta_{\mathbf{x}(t)}$ (yellow boundary), we have $\lambda > 0$, reflecting the fact that the system naturally drifts away from $\mathbf{x}(t)$. By adding control inputs, we aim to attenuate λ and push it below zero -— the point at which the dynamics naturally decay toward $\mathbf{x}(t)$ (blue arrows). Therefore, here the controllability condition is given by $f(B, \mathbf{x}(0), \mathbf{x}(t)) = 1$ if $\lambda < 0$, providing the minimal driver node set

as

$$S_{\min}^{\mathrm{C}} = \underset{S\subseteq V}{\operatorname{argmin}} \Big\{ |S| \;\Big|\; \lambda < 0 \Big\}. \tag{6}$$

Finding $S_{\min}^{\mathrm{C}}$ is thus an optimization problem, seeking the smallest set of nodes sufficient to push $\lambda < 0$.

In Supplementary Section 2.1.2, we develop an algorithmic approach to address this optimization challenge. The idea is that the most likely candidates for inclusion in $S_{\min}^{\mathrm{C}}$ are those whose addition has the greatest impact on λ. This allows us to rank nodes according to their contribution to reducing λ. We begin with an empty $S_{\min}^{\mathrm{C}}$ and iteratively add the top-ranked node to the set. After each addition, we update λ and re-rank all nodes. This process continues until $\lambda < 0$ (Fig. 4b, MLE-based).

In Fig. 4d, we track this process by plotting λ versus $|S|$ for the ER network under Kuramoto dynamics (solid blue line, MLE). At each step of the algorithm, we add the top-ranked node to S and measure the resulting change in λ. Once λ crosses below the zero line (grey dashed), we achieve the desired compatible control and identify the minimal driver node set $S_{\min}^{\mathrm{C}}$. We repeat this procedure for the Lorenz and Rössler dynamics (Fig. 4e,f), then for the scale-free network SF1 (Fig. 4g-i), and finally for all 48 network-dynamical systems (Supplementary Section 2.1.2 and Supplementary Figs. 1-4). Results for ER and SF1 are shown explicitly in Fig. 3f,j, where nodes in $S_{\min}^{\mathrm{C}}$ are highlighted in blue shades (light blue - Kuramoto, blue - Lorenz, dark blue - Rössler).

Similar to the case of incompatible control, we find, here too, that the fraction s of driver nodes depends on the degree heterogeneity. However, the nature of this dependence is now reversed. Under compatible control, s is larger for homogeneous networks and decreases with increasing network heterogeneity (Fig. 3n-p). For example, in ER we have $s = 0.81, 0.35$ and 0.82 for the three different dynamics. This is while in SF1, under the same $\mathbf{x}(0)$ and $\mathbf{x}(t)$, it is $s = 0.35, 0.1, 0.23$, an approximately three-fold reduction. A similar trend is observed in our empirical systems. For example, Brain 2, which is extremely heterogeneous, exhibits a relatively small s, but after randomization its driver node set grows almost by an order of magnitude (Fig. 3n-p, marked by arrows).

This captures our first key observation. The control profile of heterogeneous networks is selective. It is characterized by relatively easy compatible control, reflected in small s_{C}, but remains resistant to incompatible control, reflected in large s_{IC}. Thus, heterogeneity emerges as a key contributor to the functional robustness of complex systems.

To quantify this systematically, we define a system's functional robustness as

$$\phi = \frac{s_{\mathrm{IC}}}{s_{\mathrm{C}}}, \tag{7}$$

which captures the extent to which $s_{\mathrm{IC}} > s_{\mathrm{C}}$. A large ϕ indicates a significant gap between incompatible and compatible control, reflecting the system's strong functional robustness. We also measure each network's degree heterogeneity using the Fano factor[35]:

$$\rho = \frac{\sigma_k^2}{\langle k \rangle}, \tag{8}$$

which characterizes the broadness of $P(k)$. In Fig. 3q, we show ϕ versus ρ for the 48 systems in our testing ground. As predicted, ϕ increases with ρ, confirming that degree heterogeneity, indeed, enhances functional robustness.

The role of the hubs. The scale-free advantage for compatible control arises from the disproportionate dynamic influence of the hubs. Returning to our landscape analogy in Fig. 1, compatible control involves driving the system into a basin. In a degree-heterogeneous network, this can be achieved efficiently by focusing preferentially on the hubs. Once the hubs are guided into the desired basin, the low-degree nodes follow naturally through the system's endogenous dynamics. Consequently, degree-heterogeneous networks are highly susceptible to compatible control.

To observe this systematically across all networks and dynamics, in Fig. 3f-m we show $P(i \in S_{\min}^{\mathrm{C}} \mid k_i)$ versus k_i for ER and SF1 under compatible control. In contrast to incompatible control, we now observe a clear positive dependence on degree, where low-degree nodes are consistently excluded, and the hubs dominate the minimal driver node set. Similar results are observed across the remaining systems in our testing ground (Supplementary Section 2.1.3).

Degree-based construction of $S_{\min}^{\mathrm{C}}$. Our original algorithm for constructing $S_{\min}^{\mathrm{C}}$ required ranking nodes based on their contribution to the MLE λ, with the ranking updated at each iteration (Fig. 4b). We now offer

a simplified alternative based solely on degree ranking. As indicated in Fig. 3f-m, $S^{\mathrm{C}}_{\mathrm{min}}$ is strongly hub-selective, with only the highest-degree nodes included in the driver node set. We therefore rank all nodes by degree and add them one by one to $S^{\mathrm{C}}_{\mathrm{min}}$ until reaching the desired condition $\lambda < 0$ (Fig. 4c). The results of this simplified degree-based algorithm are shown in Fig. 4d-i (dashed line-squares), where we find that, for all practical purposes, it is almost indistinguishable from the more exact MLE-based algorithm (solid lines).

Our simplified degree-based algorithm provides an efficient way to obtain a well-approximated $S^{\mathrm{C}}_{\mathrm{min}}$, bypassing the computational burden of iteratively calculating λ node by node. A rigorous complexity analysis of both algorithms appears in Supplementary Section 3.

More broadly, the fact that such a simple ranking can quantitatively capture the composition of $S^{\mathrm{C}}_{\mathrm{min}}$, in itself, strongly reinforces our central insight: under compatible control, a node's degree is the primary predictor of its role as a driver node. This is, indeed, the root cause of the observed functional robustness in heterogeneous networks.

Control energy

After identifying the minimal driver node sets $S^{\mathrm{C}}_{\mathrm{min}}$ and $S^{\mathrm{IC}}_{\mathrm{min}}$, we introduce signals $\mathbf{u}(t)$, injected into the detected driver nodes, to steer the system from $\mathbf{x}(0)$ to $\mathbf{x}(t)$. The initial and final states are selected as shown in Fig. 2e-j, reflecting both compatible and incompatible control. At each time point along the system's trajectory, we measure the instantaneous control power $W(t) = ||\mathbf{u}(t)||^2$.

In Fig. 5a, we present $W(t)$ versus t for Kuramoto dynamics under compatible control. Results are shown for both ER (light blue) and SF1 (dark blue). In the limit $t \to \infty$, for both networks, we have $W(t) \to 0$, as the system enters the basin of $\mathbf{x}(t)$ and the driving signals $\mathbf{u}(t)$ can be relaxed. Crucially, however, this convergence is much more rapid for SF1, indicating that scale-free networks are more amenable to compatible control. Similar results are obtained for Lorenz (Fig. 5d) and Rössler (Fig. 5g).

The total energy E in (4) is given by the time integral of $W(t)$, *i.e.* the area under the curves in Fig. 5a,d,g. As expected, E_{C}, the compatible control energy, favors SF1 over ER – a trend observed across our entire ensemble of network-dynamics combinations (Fig. 5b,e,h, Supplementary Section 2.3). For incompatible control, the picture reverses, as observed in Fig. 5j-r. The homogeneous ER (dark red) now requires less energy than SF1 (light red).

Under incompatible control, since $\mathbf{x}(t) \notin \mathcal{M}$, energy must continue to be expended even after reaching the target state. This represents the holding energy, without which the system would eventually return to $\mathcal{M}$. In Supplementary Section 2.3, we analyze $W_{\mathrm{H}}(t)$ versus t, the energy per unit time invested near the target state $\mathbf{x}(t)$ for our three dynamical systems. There too, we show, the average $\langle W_{\mathrm{H}} \rangle$ tends to be higher for heterogeneous networks as compared to homogeneous ones.

To systematically evaluate the effect of degree heterogeneity on control energy, we use an analogous definition to (7), writing

$$\varepsilon = \frac{E_{\mathrm{IC}}}{E_{\mathrm{C}}}. \tag{9}$$

A functionally robust system requires much energy for incompatible control and little energy for compatible control, thus having $E_{\mathrm{IC}} > E_{\mathrm{C}}$ and hence a large ε. In Fig. 5s we present ε versus the network heterogeneity ρ, defined in (8), finding, once again, that heterogeneity, indeed enhances functional robustness. Similar results are observed for the holding energy, as captured by ε's counterpart metric ε_{H} (Fig. 5t, see Supplementary Section 2.3.2 for ε_{H}'s precise definition).

Taken together, our analysis shows that the umbrella term controllability encompasses two fundamentally distinct forms of control, which lead to predictably different outcomes. Under the classic notion of control, here termed incompatible, heterogeneous networks are control-averse: they require more driver nodes and greater energy to steer them toward an arbitrary target state. Crucially, however, this general claim overlooks a distinguished subset of control targets – the compatible states – for which the picture is reversed, and heterogeneity actually facilitates control.

We interpret this to mean that heterogeneous networks are functionally robust: difficult to drive *away* from their natural dynamics, yet easy to guide back *toward* them. Our findings therefore point to degree heterogeneity as a general dynamical mechanism by which complex systems confine their behavior to functional states while remaining selectively controllable within that space. In this sense, degree heterogeneity is not merely a structural

hallmark of complex systems, but a dynamical design principle that balances functional stability with adaptive flexibility.

Discussion and outlook

Our distinction between compatible and incompatible control closes a gap between the engineering notion of controllability and the physical notion of dynamical admissibility [20,36]. Classical control theory asks whether a system can be driven to a prescribed state, treating the state space as uniformly admissible. Yet in self-organized physical, biological and technological systems, large regions of this state space may be dynamically unnatural, unstable, or functionally irrelevant. In these settings, meaningful control does not constitute arbitrary state assignment, but dynamics-compatible guidance. Compatible targeting therefore asks whether perturbations can be aligned with the attractors, collective modes and feasible directions naturally ingrained within the networked dynamics.

This perspective may help explain why heterogeneous architectures are so prevalent in biological, technological and social systems. Such networks must remain adaptable to internal and external demands, yet protected against disruptive perturbations. Degree heterogeneity may contribute to this balance by separating compatible from incompatible interventions, thereby allowing the system to respond efficiently to functionally meaningful inputs while suppressing dynamically unnatural ones.

Beyond self-organized systems, our results also suggest a design principle for artificial and engineered networks. Rather than maximizing unrestricted controllability, robust network design may require identifying and exploiting compatible control channels: interventions that act with the system's intrinsic dynamics, rather than against them. Such design may be particularly relevant for biological regulation, infrastructure systems and adaptive technologies, where the goal is rarely to impose an arbitrary state, but to guide the system toward functional, stable and energetically sustainable behavior.

Our results indicate that the distinction between compatible and incompatible control is particularly pronounced for the chaotic attractors of the Lorenz and Rössler systems. This is observed in Figs. 3q and 5s,t, where the measured ϕ, ε and ε_{H} align more tightly along the linear plots for the chaotic systems, Lorenz and Rössler (orange and green), than for the non-chaotic Kuramoto dynamics (blue). One possible explanation lies in the dynamical richness of the compatible set. Under the relatively simple periodic attractor of Kuramoto, the system is confined to a limited repertoire, typically organized around a stable limit cycle. Hence, the internal structure of the compatible set $\mathcal{M}$ remains comparatively poor. By contrast, chaotic attractors contain a highly structured continuum of recurrent dynamical patterns, including embedded unstable periodic orbits. They therefore support a much richer set of admissible trajectories, combining geometric complexity with temporal diversity. Such richer organization may make the distinction between compatible and arbitrary states more informative, thereby amplifying the differences observed in their control profiles.

Our analysis focuses on structural diversity, as quantified by the parameter ρ in (8). This is motivated by the fact that degree heterogeneity captures a robust macro-level characteristic of a wide range of real-world network. Beyond ρ, however, networks present a rich set of more nuanced structural characteristics, such as degree correlations, clustering, modularity, and localization of eigenmodes. A similar analysis may uncover how these meso-scale architectures also impact the system's functional robustness.

Another limitation of the present study is that it assumes a known network A_{ij} and dynamics (1). This setting is essential for testing our hypothesis on functional robustness. We acknowledge, however, that in many practical scenarios both the network and the dynamics may be only partially observed, subject to uncertainty, or vary in time [37–39]. Extending our framework to such systems will require data-driven methodologies for inferring the admissible target manifolds and identifying energy-efficient control directions.

The discovery of scale-free phenomena played a crucial role in the inception of network science, transforming our understanding of complex systems. Our work shows that this discovery was not merely a structural observation. Rather, it underlies a deeply ingrained characteristic of complex systems, namely their remarkable capacity for functional robustness. Moreover, the fact that this connection emerges consistently across our broad testing ground suggests that it reflects a general feature of network dynamics. This generality further reinforces the view that complex systems, much like classical physical systems, are governed by universal and quantifiable principles [15,40,41].

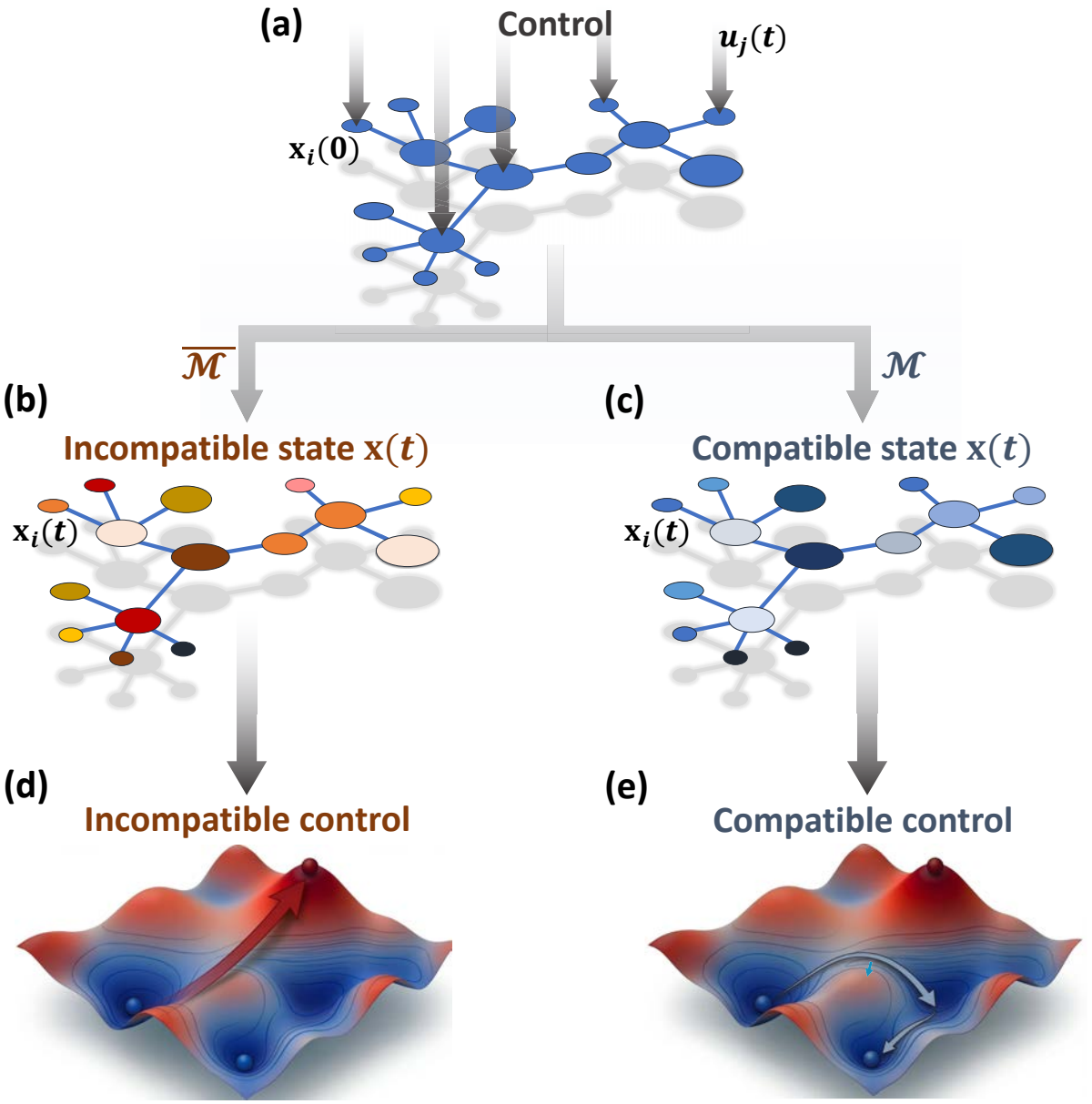


Figure 1: **Compatible vs. incompatible control.** **a** A complex network is initialized at $\mathbf{x}(0) = (\mathbf{x}_1(0), \ldots, \mathbf{x}_N(0))^\top$. Control inputs $\mathbf{u}(t)$ (arrows) are applied to selected nodes to steer the system toward a desired target state $\mathbf{x}(t)$. These target states fall into two classes: **b** Incompatible states, $\mathbf{x}(t) \in \overline{\mathcal{M}}$, are target trajectories that lie outside the system's attractor manifold $\mathcal{M}$. **c** Compatible states, $\mathbf{x}(t) \in \mathcal{M}$, lie on one of the system's natural attractors. **d** Incompatible states (red sphere) occupy peaks or ridges of the system's basin landscape. Incompatible control therefore requires pushing the system against its natural flow patterns (red arrow). **e** Compatible control drives the system into an attractor basin (blue arrows), from which it naturally flows toward the desired target state, $\mathbf{x}(t) \in \mathcal{M}$ (blue sphere). This form of control is also known as targeting.

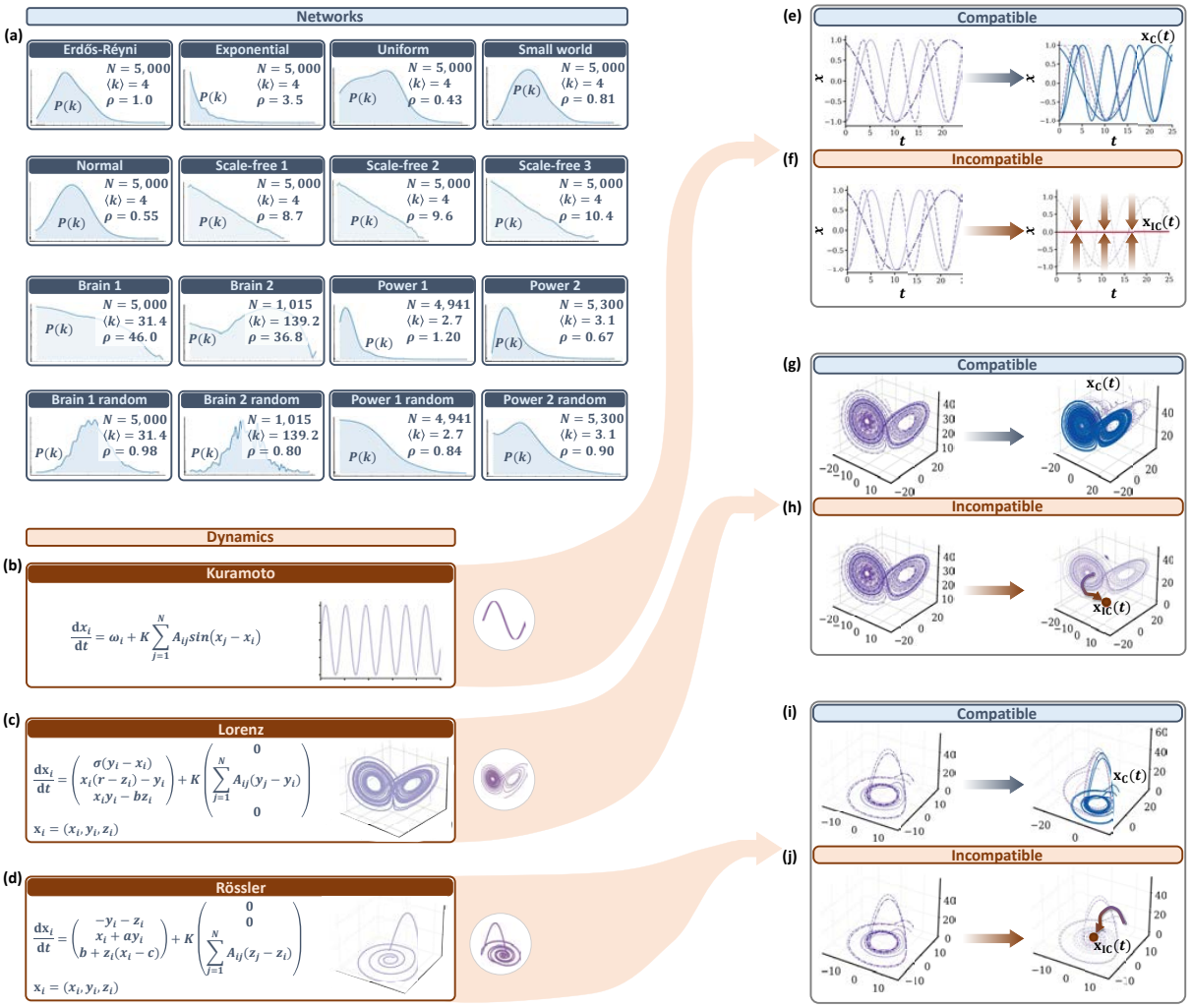


Figure 2: **Testing ground for functional robustness**. **a** We consider 16 synthetic and real-world networks. For each network, we report its size N, average degree $\langle k \rangle$, and heterogeneity score ρ in (8). The degree distribution $P(k)$ is also shown (blue). The empirical networks include two human connectomes (Brain 1 and 2) and two power transmission networks (Power 1 and 2), in both original structure and randomized. **b-d** The networks are coupled to three canonical dynamical systems: Kuramoto, Lorenz, and Rössler. For each dynamics, we show the governing equation, in the form of Eq. (1), together with the corresponding natural attractor (violet). Altogether, this yields 48 networked dynamical systems, spanning distinct attractor states and a broad range of heterogeneity levels, from $\rho = 0.43$ to $\rho = 46.0$. **e** To test compatible control for Kuramoto dynamics, we initialize the system at an arbitrary $\mathbf{x}(0)$ (left) and seek to steer it toward the phase-locked attractor state $\mathbf{x}_C(t)$ (right). **f** For incompatible control, we begin from the same initial state, but set the target state to $\mathbf{x}_{IC}(t) = 0$ (right, red). **g** Compatible control of the Lorenz system drives the dynamics toward its natural attractor (right, blue). **h** To examine incompatible control, we instead seek to pin the system to the static state $\mathbf{x}_{IC}(t)$ (right, red dot). **i-j** Compatible and incompatible control of the Rössler system.

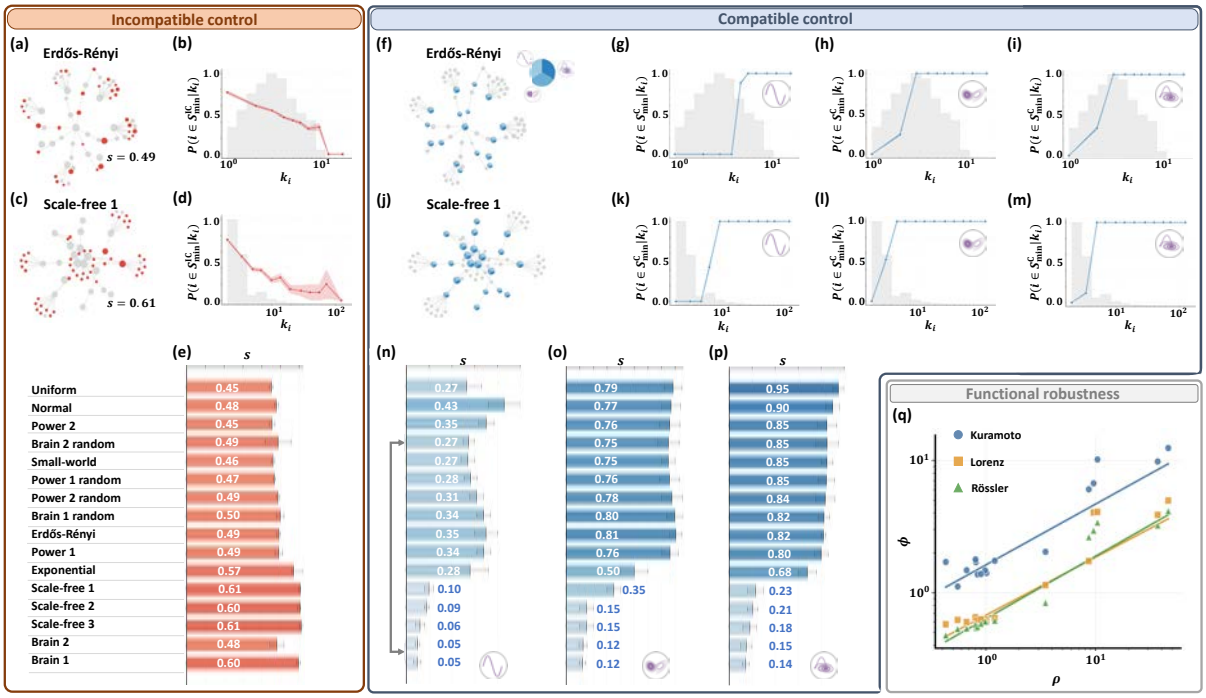


Figure 3: **The minimal driver node set under compatible and incompatible control**. **a** The minimal driver node set $S_{\min}^{\mathrm{IC}}$ obtained for the Erdős-Rényi network under incompatible control (red nodes; shown is a sample extracted from the full network). The fraction of nodes in $S_{\min}^{\mathrm{IC}}$ is $s = 0.49$, and their locations at the network periphery indicate a preference for the low-degree nodes. **b** The conditional probability $P(i \in S_{\min}^{\mathrm{IC}} \mid k_i)$ versus k_i (red). The probability declines with k_i, corroborating that incompatible control favors low-degree nodes and tends to avoid hubs. The degree distribution $P(k)$ is also shown (grey). **c** Similar results for the Scale-free 1 network, this time with $s = 0.61$. **d** Here too, $S_{\min}^{\mathrm{IC}}$ systematically avoids the hubs. **e** The fraction of driver nodes s for all 16 networks in our database. Networks are arranged from least to most heterogeneous, showing that s increases with degree heterogeneity. This is consistent with the well-known result that heterogeneous networks are difficult to control, here reaffirmed specifically for the case of incompatible control. **f** $S_{\min}^{\mathrm{C}}$ for the Erdős-Rényi network under compatible control, as obtained for Kuramoto (light blue), Lorenz (blue), and Rössler (dark blue) dynamics. The driver nodes tend to condense near the center, indicating that $S_{\min}^{\mathrm{C}}$ is composed primarily of hubs. **g-i** The conditional probability $P(i \in S_{\min}^{\mathrm{C}} \mid k_i)$ versus k_i for the three dynamics (blue). In contrast to incompatible control, here the probability shows a sharp preference for high-degree nodes. **j-m** Similar results for Scale-free 1. **n** The fraction of driver nodes s under compatible control across all networks, shown here for Kuramoto dynamics. Here, heterogeneity facilitates control, and hence more heterogeneous networks (bottom) exhibit smaller s. As an example, we highlight with a grey arrow the highly heterogeneous Brain 2 network ($\rho = 36.8, s = 0.12$), which after randomization requires a much larger driver node set ($\rho = 0.80, s = 0.75$). **o-p** We observe a similar trend also for Lorenz and Rössler dynamics. **q** Functional robustness ϕ in (7) versus network heterogeneity ρ, as obtained from Kuramoto (blue), Lorenz (orange) and Rössler (green) dynamics, implemented on each of our 16 networks. A clear trend emerges, whereby heterogeneous networks exhibit enhanced functional robustness.

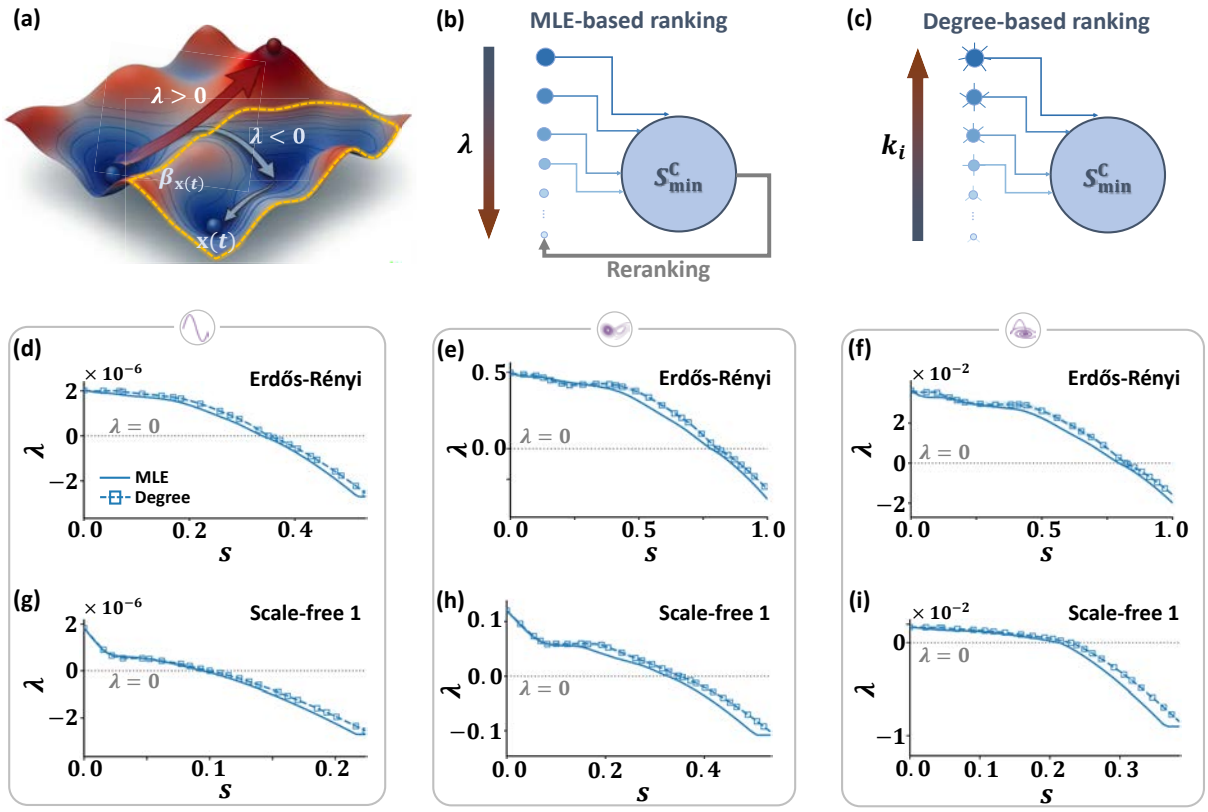


Figure 4: **Constructing the minimal driver node set $S^{\mathrm{C}}_{\mathrm{min}}$ for compatible control.** **a** Under compatible control, the system must be steered into the basin of attraction $\beta_{\mathbf{x}(t)}$ (yellow boundary) of the target state $\mathbf{x}(t)$ (blue sphere). Once within this range, the system's internal dynamics naturally drive it toward the desired target (blue arrows). This is captured by the maximum Lyapunov exponent (MLE) λ, which is positive for trajectories outside $\beta_{\mathbf{x}(t)}$ (red arrow) and becomes negative once the system enters the desired basin. Therefore, to construct $S^{\mathrm{C}}_{\mathrm{min}}$ we seek the minimal set of nodes for which $\lambda < 0$. **b** MLE-based algorithm. We rank all nodes according to their contribution to reducing λ. We then introduce the top-ranked node into $S^{\mathrm{C}}_{\mathrm{min}}$ and re-rank the remaining nodes. The process terminates once $\lambda < 0$. **c** Degree-based algorithm. We also consider an approximate algorithm in which nodes are introduced into $S^{\mathrm{C}}_{\mathrm{min}}$ based on degree alone. This alternative constructs $S^{\mathrm{C}}_{\mathrm{min}}$ directly from the network topology, allowing us to bypass the re-ranking process after each iteration. **d** λ versus the fraction of nodes s introduced into $S^{\mathrm{C}}_{\mathrm{min}}$ for the Erdős-Rényi network with Kuramoto dynamics, as obtained from the MLE-based algorithm (solid line). As nodes are added, λ decreases until it crosses the $\lambda = 0$ line (grey dashed), at which point no additional nodes are required and the minimal set is complete. We also show the results from the degree-based approach (squares), which are nearly indistinguishable. **e-i** Similar results for Lorenz and Rössler dynamics, and for Scale-free 1.

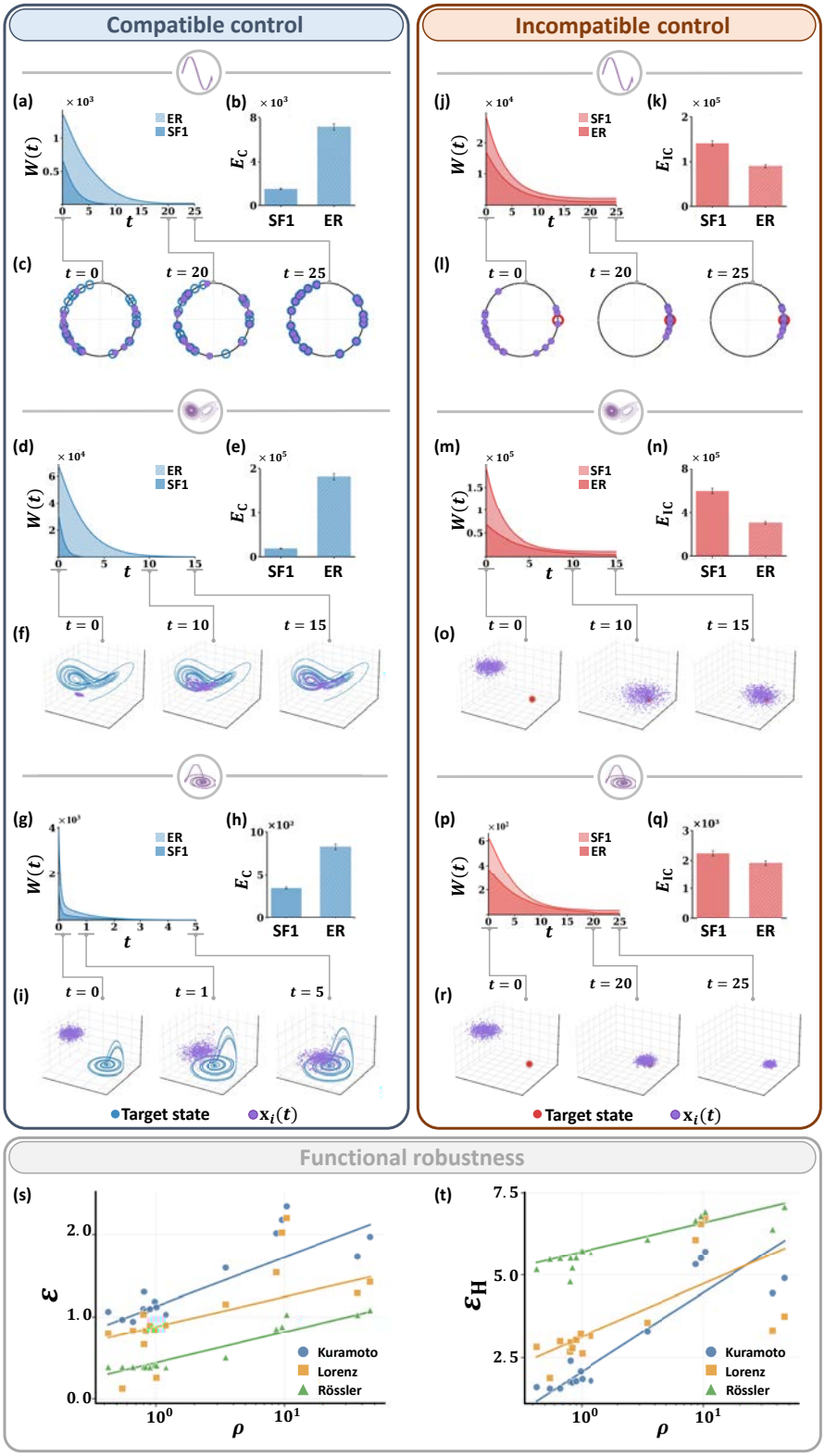


Figure 5: **Control energy**. We implemented compatible (blue) and incompatible (red) control across all networked dynamical systems, using the initial and target states shown in Fig. 2e-j. **a** Power $W(t)$ versus t along the compatible control trajectory for the Erdős-Rényi (light blue) and Scale-free 1 (dark blue) networks with Kuramoto dynamics. The area under each curve represents the total control energy. **b** Compatible control energy E_C is lower for Scale-free 1 than for Erdős-Rényi. **c** Three snapshots at selected time points along the trajectory from $\mathbf{x}(0)$ to $\mathbf{x}(t)$. Shown are the phases of selected nodes at time t ($\mathbf{x}_i(t)$, purple circles) and at the target state (blue circles). At $t = 25$, the blue and purple circles coincide, indicating that the system has reached the target state. **d-i** Similar results for Lorenz and Rössler dynamics. **j-q** For incompatible control, the trend reverses: Scale-free 1 now requires more energy than Erdős-Rényi. Here the target states are shown in red. **s** Functional robustness ε in (9) vs. ρ in (8) for Kuramoto (blue) Lorenz (orange) and Rösller (green). As predicted, robustness increases with network heterogeneity. **t** Similar results for the holding energy in incompatible control (Supplementary Section 2.3).

References

[1] Strogatz, S. H. Exploring complex networks. *Nature* **410**, 268–276 (2001).

[2] Barabási, A. L., & Albert, R. Emergence of scaling in random networks. *Science* **286**, 509–512 (1999).

[3] Serafino, M., Cimini, G., Maritan, A., Rinaldo, A., Suweis, S., Banavar, J. R., & Caldarelli, G. True scale-free networks hidden by finite size effects. *Proc. Nat. Acad. Sci.* **118**, e2013825118 (2021).

[4] Jeong, H., Tombor, B., Albert, R., Oltvai, Z. N., & Barabási, A. L. The large-scale organization of metabolic networks. *Nature* **407**, 651–654 (2000).

[5] Zhou, B., Holme, P., Gong, Z., Zhan, C., Huang, Y., Lu, X., & Meng, X. The nature and nurture of network evolution. *Nat. Commun.* **14**, 7031 (2023).

[6] Blumenthal, D. B., Lucchetta, M., Kleist, L. et al. Emergence of power law distributions in protein-protein interaction networks through study bias. *Elife* **13**, e99951 (2024).

[7] Hu, X., Dong, G., Christensen, K. et al. Unveiling the importance of nonshortest paths in quantum networks. *Sci. Adv.* **11**, eadt2404 (2025).

[8] Battiston, F., Cencetti, G., Iacopini, I. et al. Networks beyond pairwise interactions: Structure and dynamics. *Phys. Rep.* **874**, 1–92 (2020).

[9] Duan, C., Nishikawa, T., Eroglu, D., & Motter, A. E. Network structural origin of instabilities in large complex systems. *Sci. Adv.* **8**, eabm8310 (2022).

[10] Sun, H. et al. Network controllability of structural connectomes in the neonatal brain. *Nat. Commun.* **14**, 5820 (2023).

[11] Battiston, F. et al. The physics of higher-order interactions in complex systems. *Nat. Phys.* **17**, 1093–1098 (2021).

[12] Albert, R., Jeong, H., & Barabási, A. L. Error and attack tolerance of complex networks. *Nature* **406**, 378–382 (2000).

[13] Artime, O. et al. Robustness and resilience of complex networks. *Nat. Rev. Phys.* **6**, 114–131 (2024).

[14] Cohen, R., Erez, K., Ben-Avraham, D., & Havlin, S. Resilience of the internet to random breakdowns. *Phys. Rev. Lett.* **85**, 4626 (2000).

[15] Barzel, B., & Barabási, A. L. Universality in network dynamics. *Nat. Phys.* **9**, 673–681 (2013).

[16] Gao, J., Barzel, B., & Barabási, A. L. Universal resilience patterns in complex networks. *Nature* **530**, 307–312 (2016).

[17] Sanhedrai, H., Gao, J., Bashan, A., Schwartz, M., Havlin, S., & Barzel, B. Reviving a failed network through microscopic interventions. *Nat. Phys.* **18**, 338–349 (2022).

[18] Liu, Y.-Y., Slotine, J.-J., & Barabási, A.-L. Controllability of complex networks. *Nature* **473**, 167–173 (2011).

[19] Lin, C. T. Structural controllability. *IEEE Trans. Autom. Control* **19**, 201–208 (1974).

[20] D'Souza, R. M., Di Bernardo, M., & Liu, Y. Y. Controlling complex networks with complex nodes. *Nat. Rev. Phys.* **5**, 250–262 (2023).

[21] Gutiérrez, R., Sendina-Nadal, I., Zanin, M., Papo, D., & Boccaletti, S. Targeting the dynamics of complex networks. *Sci. Rep.* **2**, 396 (2012).

[22] Meena, C., Hens, C., Acharyya, S., Haber, S., Boccaletti, S., & Barzel, B. Emergent stability in complex network dynamics. *Nat. Phys.* **19**, 1033–1042 (2023).

[23] Bi, M.-X., Fan, H., Yan, X.-H. & Lai, Y.-C. Folding state within a hysteresis loop: Hidden multistability in nonlinear physical systems. *Phys. Rev. Lett.* **132**, 137201 (2024).

[24] Kong, L.-W., Brewer, G. A. & Lai, Y.-C. Reservoir-computing based associative memory and itinerancy for complex dynamical attractors. *Nat. Commun.* **15**, 4840 (2024).

[25] Shinbrot, T., Grebogi, C., Yorke, J. & Ott, E. Using small perturbations to control chaos. *Nature* **363**, 411–417 (1993).

[26] Shinbrot, T., Ditto, W., Grebogi, C., Ott, E., Spano, M., & Yorke, J. A. Using the sensitive dependence of chaos (the "butterfly effect") to direct trajectories in an experimental chaotic system. *Phys. Rev. Lett.* **68**, 2863 (1992).

[27] Rossi, R., & Ahmed, N. The network data repository with interactive graph analytics and visualization. *Proc. AAAI Conf. Artif. Intell.* **29** (2015).

[28] Szalkai, B., Kerepesi, C., Varga, B., & Grolmusz, V. The Budapest reference connectome server v2.0. *Neurosci. Lett.* **595**, 60–62 (2015).

[29] Watts, D. J., & Strogatz, S. H. Collective dynamics of 'small-world' networks. *Nature* **393**, 440–442 (1998).

[30] Davis, T. A., & Hu, Y. The University of Florida sparse matrix collection. *ACM Trans. Math. Softw.* **38**, 1–25 (2011).

[31] Kalman, R. E. Mathematical description of linear dynamical systems. *J. Soc. Ind. Appl. Math.* **1**, 152–192 (1963).

[32] Hopcroft, J. E., & Karp, R. M. An $n^{5/2}$ algorithm for maximum matchings in bipartite graphs. *SIAM J. Comput.* **2**, 225–231 (1973).

[33] Wolf, A., Swift, J. B., Swinney, H. L., & Vastano, J. A. Determining Lyapunov exponents from a time series. *Physica D* **16**, 285–317 (1985).

[34] Ott, E., Grebogi, C., & Yorke, J. A. Controlling chaos. *Phys. Rev. Lett.* **64**, 1196 (1990).

[35] Fano, U. Ionization yield of radiations. II. The fluctuations of the number of ions. *Phys. Rev.* **72**, 26 (1947).

[36] Jiang, J. & Lai, Y.-C. Irrelevance of linear controllability to nonlinear dynamical networks. *Nat. Commun.* **10**, 3961 (2019).

[37] MacLaren, N. G., Barzel, B. & Masuda, N. Observing network dynamics through sentinel nodes. *Nat. Commun.* **16**, 10211 (2025).

[38] Prasse, B. & Van Mieghem, P. Predicting network dynamics without requiring the knowledge of the interaction graph. *Proc. Nat. Acad. Sci.* **119**, e2205517119 (2022).

[39] Di Gaetano, L., Battiston, F. & Starnini, M. Percolation and topological properties of temporal higher-order networks. *Phys. Rev. Lett.* **132**, 037401 (2024).

[40] Thibeault, V., Allard, A., & Desrosiers, P. The low-rank hypothesis of complex systems. *Nat. Phys.* **20**, 294–302 (2024).

[41] Gabrielli, A., Garlaschelli, D., Patil, S. P. & Serrano, M. Á. Network renormalization. *Nat. Rev. Phys.* **7**, 203–219 (2025).

Full size figures

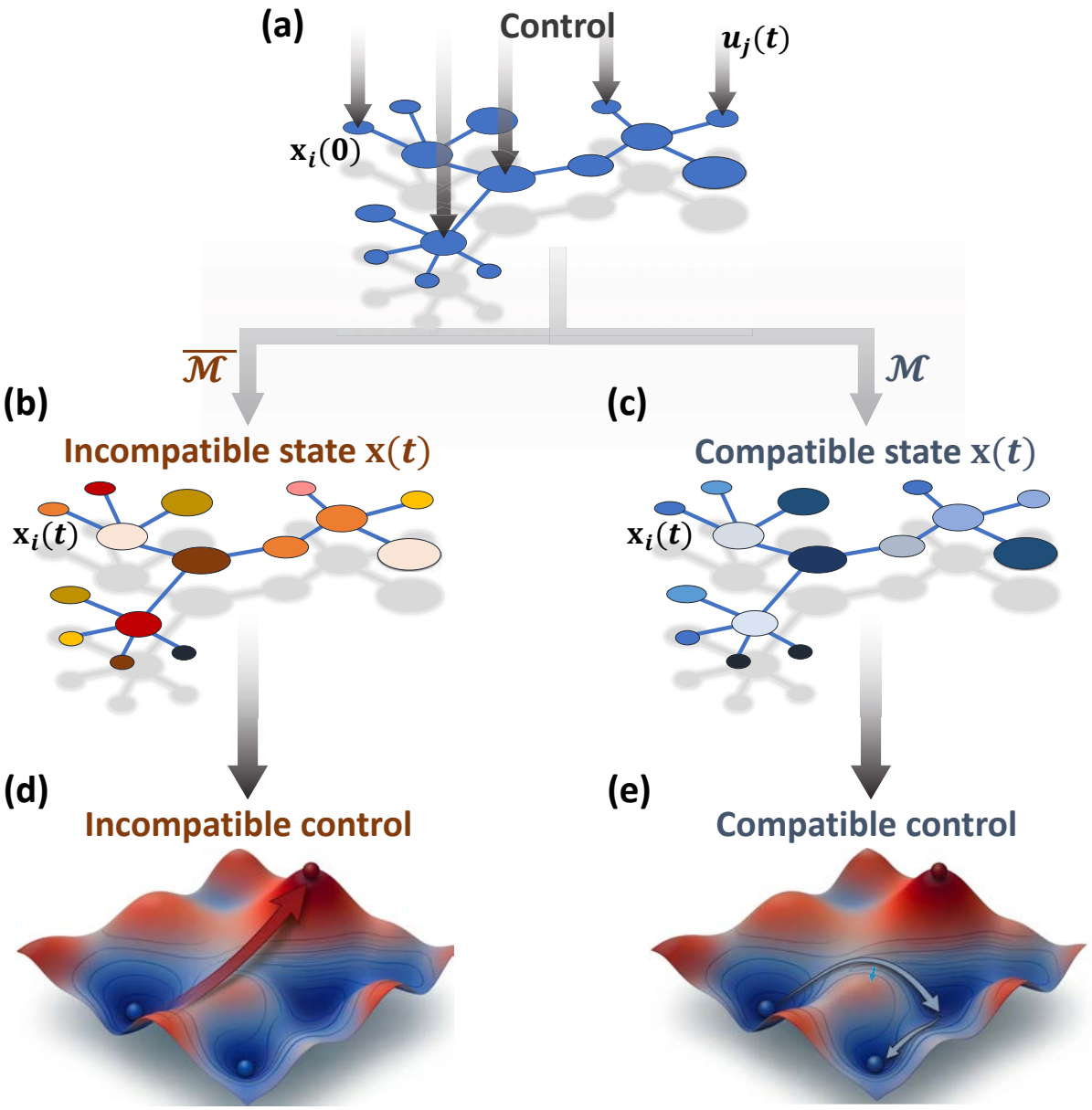


Figure 1. Compatible vs. incompatible control.

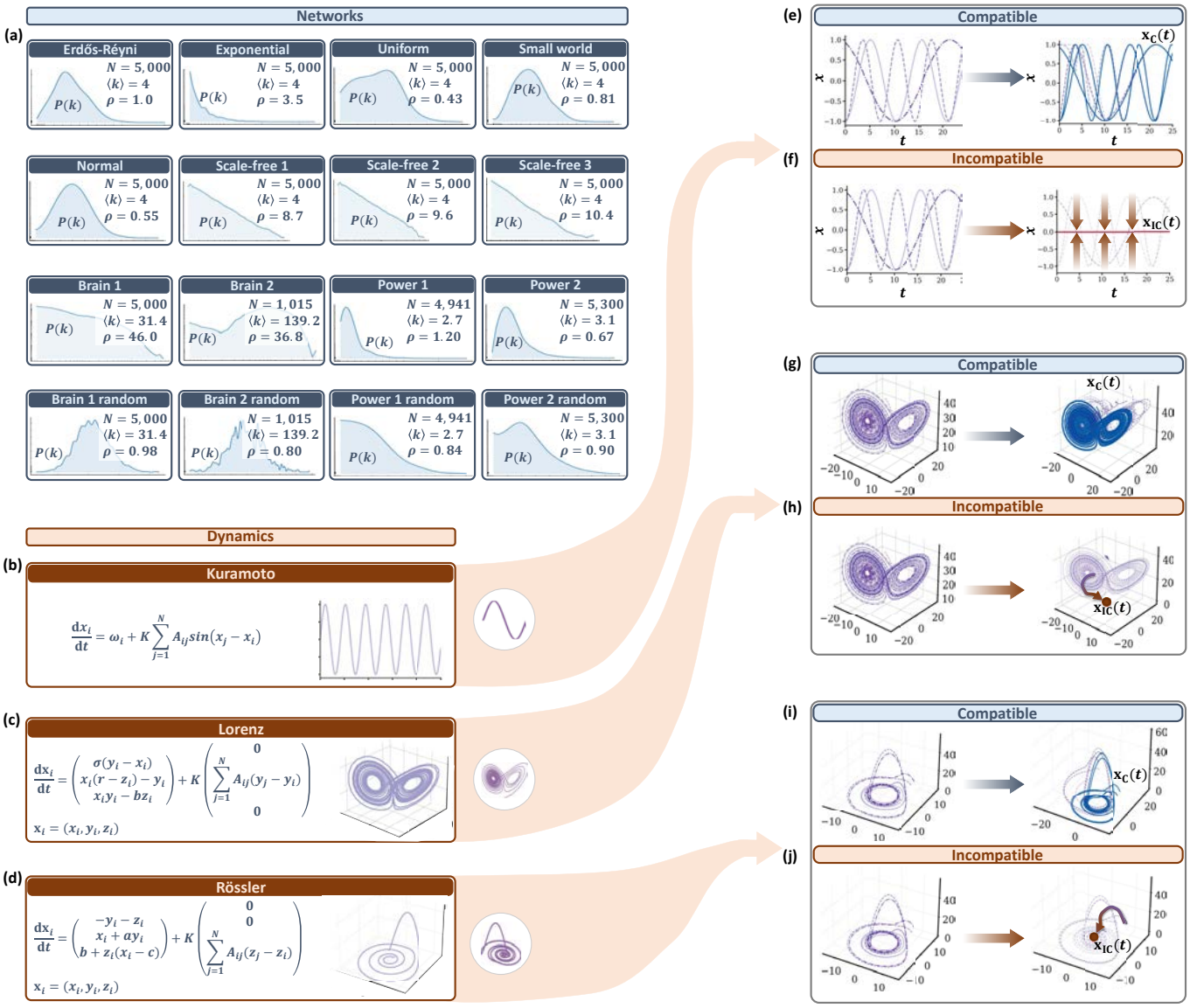


Figure 2. Testing ground for functional robustness.

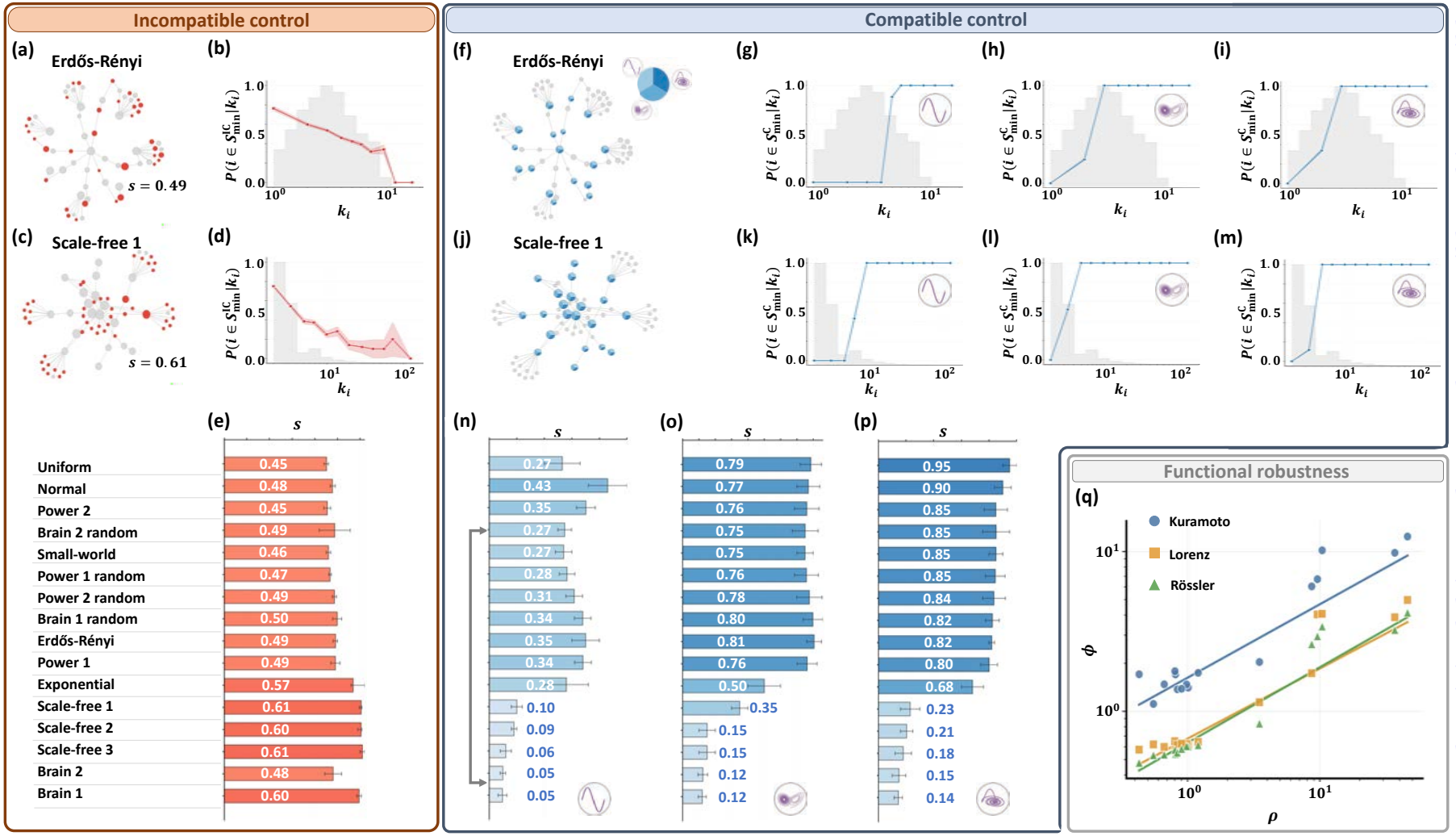


Figure 3. The minimal driver node set under compatible and incompatible control.

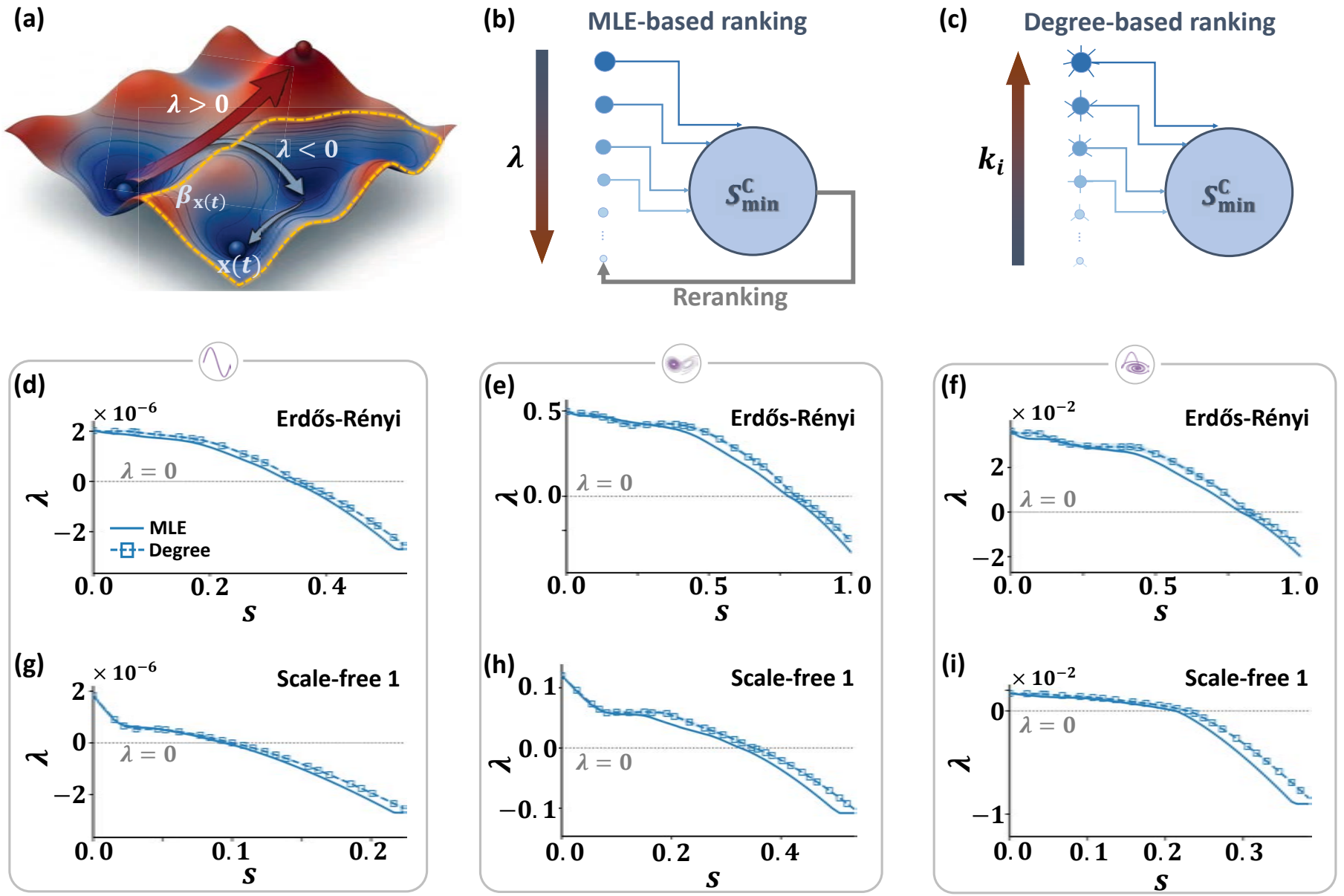


Figure 4. Constructing the minimal driver node set S^C_{min} for compatible control.

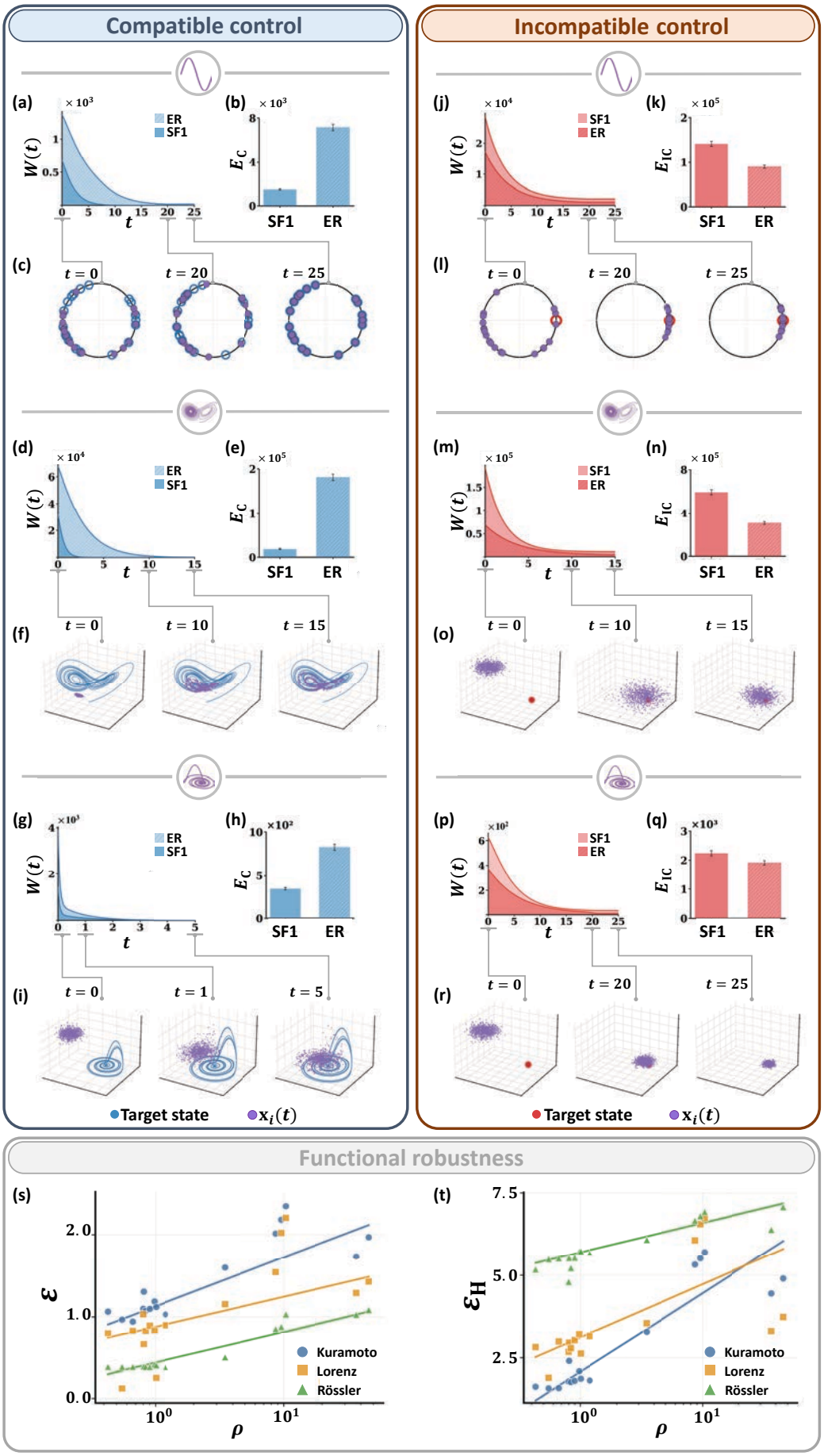


Figure 5. Control energy.

Supplementary Files

This is a list of supplementary files associated with this preprint. Click to download.

- Supplementaryfile.pdf